Bioactive Materials 12 (2022) 169–184

Contents lists available at ScienceDirect

Bioactive Materials

journal homepage: www.keaipublishing.com/en/journals/bioactive-materials

Local bone metabolism balance regulation via double-adhesive hydrogel for fixing orthopedic implants

Wei Jiang [a,1], Fushan Hou [b,1], Yong Gu [a,1], Qimanguli Saiding [c], Pingping Bao [d], Jincheng Tang [a], Liang Wu [a], Chunmao Chen [a], Cailiang Shen [e], Catarina Leite Pereira [f,g], Marco Sarmento [h], Bruno Sarmento [f,g,**], Wenguo Cui [c,*], Liang Chen [a,***]

[a] Department of Orthopaedic Surgery, Orthopedic Institute, The First Affiliated Hospital of Soochow University, 708 Renmin Rd, Suzhou, Jiangsu, 215006, PR China
[b] Department of Orthopedics, The Second Hospital of Shanxi Medical University, No. 382 Wuyi Road, Taiyuan, Shanxi, 030001, PR China
[c] Department of Orthopaedics, Shanghai Key Laboratory for Prevention and Treatment of Bone and Joint Diseases, Shanghai Institute of Traumatology and Orthopaedics, Ruijin Hospital, Shanghai Jiao Tong University School of Medicine, 197 Ruijin 2nd Road, Shanghai, 200025, PR China
[d] Department of Electrocardiography, The First Affiliated Hospital of Anhui Medical University, 218 Jixi Road, Shushan District, Hefei, Anhui, 230022, PR China
[e] Department of Orthopedics, The First Affiliated Hospital of Anhui Medical University, 218 Jixi Road, Shushan District, Hefei, Anhui, 230022, PR China
[f] i3S – Instituto de Investigação e Inovação em Saúde and INEB – Instituto de Engenharia Biomédica, Universidade do Porto, Rua Alfredo Allen 208, 4200-393, Porto, Portugal
[g] CESPU - Institute for Research and Advanced Training in Health Sciences and Technologies, Rua Central de Gandra 1317, 4585-116, Gandra, Portugal
[h] Faculty of Medicine, Universidade de Lisboa, Avenida Professor Egas Moniz, 1649-028, Lisboa, Portugal

ARTICLE INFO

Keywords:
Hydrogels
Osteoporosis
Osseointegration
Dual-functional
Peri-implant

ABSTRACT

The effective osteointegration of orthopedic implants is a key factor for the success of orthopedic surgery. However, local metabolic imbalance around implants under osteoporosis condition could jeopardize the fixation effect. Inspired by the bone structure and the composition around implants under osteoporosis condition, alendronate (A) was grafted onto methacryloyl hyaluronic acid (H) by activating the carboxyl group of methacryloyl hyaluronic acid to be bonded to inorganic calcium phosphate on trabecular bone, which is then integrated with aminated bioactive glass (AB) modified by oxidized dextran (O) for further adhesion to organic collagen on the trabecular bone. The hybrid hydrogel could be solidified on cancellous bone *in situ* under UV irradiation and exhibits dual adhesion to organic collagen and inorganic apatite, promoting osteointegration of orthopedic implants, resulting in firm stabilization of the implants in cancellous bone areas. *In vitro*, the hydrogel was evidenced to promote osteogenic differentiation of embryonic mouse osteoblast precursor cells (MC3T3-E1) as well as inhibit the receptor activator of nuclear factor-κ B ligand (RANKL)-induced osteoclast differentiation of macrophages, leading to the upregulation of osteogenic-related gene and protein expression. In a rat osteoporosis model, the bone-implant contact (BIC) of the hybrid hydrogel group increased by 2.77, which is directly linked to improved mechanical stability of the orthopedic implants. Overall, this organic-inorganic, dual-adhesive hydrogel could be a promising candidate for enhancing the stability of orthopedic implants under osteoporotic conditions.

1. Introduction

Implants are unique functional materials that are planted, buried, or fixed to a damaged part of human body to provide mechanical support, or replace functionally [1]. At present, implants are mainly used in artificial organ reconstruction, surgical repair, joint replacement and

Peer review under responsibility of KeAi Communications Co., Ltd.
* Corresponding author.
** Corresponding author. i3S – Instituto de Investigação e Inovação em Saúde and INEB – Instituto de Engenharia Biomédica, Universidade do Porto, Rua Alfredo Allen 208, 4200-393, Porto, Portugal.
*** Corresponding author.
E-mail addresses: bruno.sarmento@ineb.up.pt (B. Sarmento), wgcui80@hotmail.com (W. Cui), chenliang1972@sina.com (L. Chen).
[1] These authors contributed equally to this work.

https://doi.org/10.1016/j.bioactmat.2021.10.017
Received 26 August 2021; Received in revised form 5 October 2021; Accepted 14 October 2021
Available online 19 October 2021

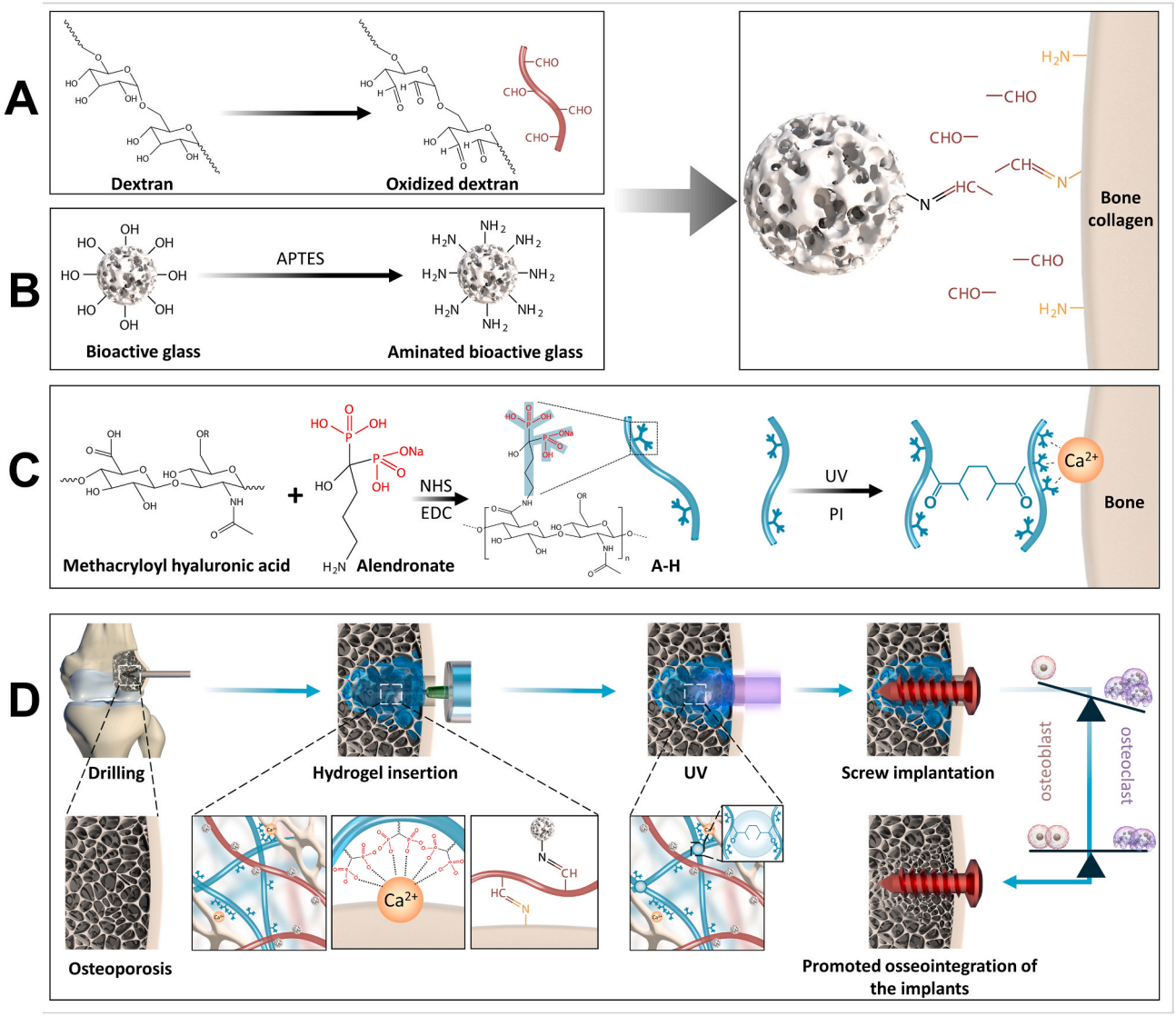

Scheme 1. Schematic illustration of double-adhesive hydrogel for Fixing Orthopedic Implants. A) Synthesis of oxidized dextran; B) Synthesis of AB; C) Synthesis of A-H; D) Fixing orthopedic implants and promoting cancellous bone reconstruction via regulating local bone metabolism in animal experiment.

other related fields [2,3]. However, the lack of biological fixation at the implant-tissue interface results in their separation, thus affecting the implantation effect [4,5]. Orthopedic implants, including bone nails, plates, pins and hybrid implants, play a crucial role in temporary fixation at fractures or lesions sites, facilitating bone repair [6]. However, these type of approaches can further contribute to weaken the bone, when osteoporotic. Early loosening of implants generally ends in failed fixation surgery [7]. Novel strategies to address the successful osseointegration between cancellous bone and implants under osteoporotic conditions represent a major unmet clinical need [8].

After orthopedic implantation, a local bone metabolism imbalance occurs due to the overactive osteoclasts making structural changes in the trabecular (porosity) and a reduction in bone composition (both organic and inorganic) around the implants [9,10]. Under this circumstances, the loose and porous condition will cause a gap between the implant and bone tissue, leading to micromotion of the implant [11]. At the same time, the reduction of organic and inorganic components in the bone matrix further hinders osseointegration of the "implanting interface" [12]. To balance the local bone metabolism under osteoporotic conditions and meet bone structural as well as compositional requirements is crucial for solving the implant loosening problem [13].

Alendronate sodium is an essential member of the bisphosphonates (BPs) family and has been widely used as the first-line therapy for osteoporosis. The R1 side chain in alendronate sodium is related to the bone affinity, while the R2 is the primary determinant of the anti-resorptive potency [14,15]. Recent studies demonstrated that a local delivery of BPs can enhance peri-implant bone density and fixation of implants [16,17].

Biomaterials, namely hydrogels that present high water contents, good biocompatibility and mechanical properties are excellent candidates as to promote local bone repair [18–20]. Currently, different chemical modifications of BPs can be introduced in hydrogels to achieve their *in situ* adhesion and solidification, thus filling loose trabecular bone structures [21,22]. Though the single component release and unilaterally inhibition of osteoclasts can promote the reconstruction of cancellous bone, there is a strong bone metabolism imbalance in osteoporotic areas, which makes it difficult to control the microenvironment of cancellous bone [22,23]. Moreover, currently published studies loaded alendronate into hydrogels are mostly lack of effective adhesion to the surrounding bone tissue, which might be flushed by body fluid and thus influence the osseointegration around the implants [21,22,24]. Previous studies have been able to demonstrate that hydrogels able to regulate local bone metabolism around intraosseous implants under osteoporotic conditions should meet the following requirements: (1). Coagulation in

the cancellous bone area [25]; (2). Integration with calcium phosphate-based inorganic substances [22]; (3). Combining with organic collagen tissue; (4). Promoting osteogenesis and inhibiting bone resorption [24]; (5). Certain interface affinity [26].

In this study, inspired by the complex and multifarious metabolic microenvironment of osteoporotic bone surrounded by the implants, an organic-inorganic, double-adhesive hydrogel that can: 1) promote osteogenesis; 2) inhibit bone resorption and 3) regulate local bone metabolism, was constructed to fix orthopedic implants under osteoporotic conditions. For that purpose, alendronate sodium was grafted onto methacryloyl hyaluronic acid (A-H) by activating the carboxyl group bonded to the inorganic calcium phosphate component of trabecular bone; further, aminated bioactive glass modified by oxidized dextran (AB-O) was chosen to bind to the organic collagen components of the trabecular bone. The hybrid hydrogel exhibited excellent injectability and biocompatibility. After UV cross-linking, it adhered and solidified *in situ*, filling the loose trabecular structure of bone, promoting osteogenesis and inhibiting bone resorption. *In vitro*, it could promote the proliferation of MC3T3-E1 and inhibit the osteoclast differentiation of macrophages induced by RANKL. In a rat osteoporosis model, this hybrid hydrogel showed the capability to significantly enhance interface osteogenesis around the implants, improve the generation of new bone and the mechanical stability of the implants (Scheme 1). Finally, histological analysis further confirmed the hydrogel's capabilities in balancing the bone metabolism around the implants *in situ*.

2. Materials and methods

2.1. Synthesis of oxidized dextran

5 g dextran (Aladdin, Shanghai) was dissolved in 100 ml of deionized water (DI water), and 5 g of sodium periodate (SINOPHARM Chemical Ltd, Shanghai) was dissolved in 60 ml of DI water. The sodium periodate solution was added to the dextran solution protected from light, and the mixture was stirred. Then, the mixture, was magnetically stirred and allowed to react for 6 h. One milliliter ethylene glycol was added to the system to stop the oxidation reaction. Subsequently, the reacted mixture was transferred to a dialysis bag with a molecular weight of 3500 and kept in deionized water for 48 h for dialysis. The DI water was replaced every 12 h. After dialysis was completed, the product was filtered with filter paper and placed at −20 °C in the refrigerator, followed by the 48 h' freeze-drying to obtain the dry aldehyde dextran powder, denoted as O in this manuscript (Table S1).

2.2. Synthesis of AB

Bioactive glass (BG, porous microspheres of 45S5 bio-glass with an average diameter of 20–50 μm) was purchased from MERYER (Shanghai). The BG (400 mg) was added to 100 ml hexane, and the mixture was shaken. Then, 5 ml (3-Aminopropyl) triethoxysilane (APTES, Sigma, USA) was added to the mixture and stirred for 24 h at 60 °C. Finally, the product was washed with alcohol and DI water 3 times to obtain the aminated bioactive glass named AB in this manuscript.

2.3. Synthesis of A-H

According to the previous research [27], alendronate (J&K, Scientific LTD) was coupled with methacryloyl hyaluronic acid (EFL, EFL-methacryloyl hyaluronic acid-400K, Suzhou, China) by using N-hydroxysuccinimide (NHS, Aladdin, Shanghai) and 1-ethyl-3-(3-dimethylaminopropyl) carbodiimide hydrochloride (EDC, Aladdin, Shanghai) as coupling agents. Briefly, 300 mg EDC, 150 mg NHS, and 500 mg methacryloyl hyaluronic acid were dissolved in 100 mL PBS (pH 5.0) with consistent stirring for 3 h. Then, 500 mg alendronate sodium was added into the solution with consistent stirring for another 3 days. Finally, the obtained product was dialyzed in the DI water with a dialysis bag (MW: 3000) for 3 days, followed by the freeze-drying process.

2.4. Preparation of the double-bonded hydrogel

Following previous protocols [28], 20 mg O and 30 mg AB were dissolved in 0.25 ml photoinitiator. The solution was ultrasonically heated at 50 °C and shaken for 0.5 h until the solution became yellow. 10 mg A-H was dissolved in 0.25 ml photoinitiator, and the solution was stirred following ultrasonication for 0.5 h to allow A-H to fully dissolve. The above two solutions were physically mixed, and the hybrid hydrogel that could be cross-linked by UV was obtained.

2.5. Weight loss and swelling test

The hydrogel was prepared in the form of disks with 5 mm diameter and 2 mm thickness. The weight of the disks after lyophilization were recorded (W_0). Then, disks were soaked in PBS for 7, 14, and 28 days at 37 °C and weighed at each time point after washing and lyophilization (W_t.). Weight loss ratio=$(W_0-W_t)/W_0*100\%$. Each experiment was repeated three times with three parallel samples (n = 3). For the swelling test, hydrogels were processed as the above-mentioned procedures and the swelling ratio calculated based on the formula: swelling percentage =$(W_t-W_0)/W_0*100\%$. Each experiment was repeated three times with three parallel samples (n = 3).

2.6. Mechanical testing

The compression tests were performed on disk samples (5 mm diameter and 2 mm thickness), which were subjected to a strain rate of 20% strain per minute on a mechanical testing machine (Shanghai Hengyi Precision Instruments Co, China). The stress models were calculated with the linear segment of the stress-strain curve. Each experiment was repeated three times with three parallel samples (n = 3).

2.7. Ion release

The A-H + AB-O hydrogel disks were soaked in simulated body fluid (SBF) for 12, 24, 48, 72, and 128 h. The SBF supernatant was collected to determine the concentrations of silicon, phosphorus and calcium by inductively coupled plasma atomic emission spectroscopy (ICP-AES, PerkinElmer Optima 7300, Waltham, MA, USA). Each experiment was repeated three times with three parallel samples (n = 3).

2.8. Cell compatibility evaluation

For the cytocompatibility testing, hydrogel sheets of all groups were spread over 24-well plates, sterilized by cobalt-60 irradiation, and exposed to 10% fetal bovine serum (FBS, Gibco, USA). The samples were soaked overnight in Minimum Essential Medium (MEM, HyClone, GE Life Sciences, USA). The mouse-derived pre-osteoblast cell line (MC3T3-E1, Procell, Wuhan, China) and bone marrow macrophages (BMMs) were seeded on the hydrogel sheets at a density of 2×10^4 cells/well and incubated at 37 °C, 95% relative humidity and 5% carbon dioxide. A live/dead staining kit ((Invitrogen, USA)) was used to stain the cells cultured for 3 days. The cells were cultured for 1, 3, and 5 days using the CCK-8 staining kit (Dojindo, Japan) for quantitative comparison. Each experiment was repeated three times with three parallel samples (n = 3).

2.9. Osteogenesis evaluation

After 7 days' culture in Transwell plates, MC3T3-E1 cells were stained with alkaline phosphatase (ALP) staining kit (Cyagen, Guangzhou, China). After 21 days' culture, MC3T3-E1 cells were stained with an alizarin red staining kit (Cyagen, Guangzhou, China). After that, the stained mineralized nodules were dissolved in perchloric acid, and the

Table 1
Primer sequences used for gene expression by RT-qPCR.

Primer name	Orientation	Sequence (5′-3′)
RUNX2	Forward	TGATGAGAACTACTCCGCC
	Reverse	GTGAAACTCTTGCCTCGTC
OCN	Forward	CTACCTTGGAGCCTCAGTC
	Reverse	TTAAGCTCACACTGCTCCC
OPN	Forward	GGTGAAAGTGACTGATTCTGG
	Reverse	GAGGACACAGCATTCTGTG
GAPDH	Forward	ACTCTTCCACCTTCGATGC
	Reverse	CCGTATTCATTGTCATACCAGG
MMP-9	Forward	GTCCAGACCAAGGGTACAG
	Reverse	ATACAGCGGGTACATGAGC
C-FOS	Forward	GAACGGAATAAGATGGCTGC
	Reverse	TTGATCTGTCTCCGCTTGG
NFATc1	Forward	ACTATGAGACGGAAGGCAG
	Reverse	CCAAGTAACCGTGTAGCTG
actin	Forward	GAAGATCAAGATCATTGCTCCT
	Reverse	CATCCACATCTGCTGGAAGG

absorbance of the solution was measured at 420 nm. Each experiment was repeated three times with three parallel samples (n = 3). Immunofluorescence staining was used to explore the osteogenic induction properties of hydrogels. After co-culture with hydrogels for different durations, the MC3T3-E1 cells were fixed with 4% paraformaldehyde for 20 min and permeabilized with 0.3% Triton-X (Aladdin, Shanghai, China) for 10 min. After that, cells were blocked with bovine serum albumin (5%, w/v) (BSA, Biosharp, Shanghai, China) overnight. Then these cells were incubated with primary antibodies against runt-related transcription factor 2 (RUNX2, Novus, USA) and osteocalcin (OCN, Novus, USA) followed by incubation with secondary antibody conjugated with fluorescent labels (Jackson, USA). After washing three times with PBS, the cells were stained with phalloidin (Yearsen, China) and 4′,6-diamidino-2-phenylindole hydrochloride (DAPI, Abcam, USA). Finally, these cells were observed by a fluorescence microscope.

Hydrogels were placed on the upper chamber of a 6-well transwell culture plate (Corning, USA), and 3×10^5 MC3T3-E1 cells were seeded on the lower chamber. After 7 days and 14 days' co-culture, the supernatant was collected and analyzed by enzyme linked immunosorbent assay (ELISA, MultiSciences, LiankeBio, China). In addition, cells were harvested from the lower chamber for the real-time quantitative real-time (RT-qPCR) to evaluate the expression of osteogenic genes, including RUNX2, OCN, and osteopontin (OPN). Glyceraldehyde-3-phosphate dehydrogenase (GAPDH) was used as an internal reference. The primer sequence was designed by Genewiz, as shown in Table 1. Each experiment was repeated three times with three parallel samples (n = 3).

2.10. Osteoclast evaluation

The BMMs were obtained from the tibia and femur of mice following a previously described protocol [29]. BMMs were cultured in Dulbecco's modified Eagle's medium (DMEM, Gibco, USA), 10% FBS, 100 U/ml penicillin (Gibco, USA) and M-CSF (30 ng/ml) (R&D, USA) for 12 h. The hydrogel sheets were placed in the upper chamber and the BMMs were collected in the lower chamber of transwell plates. RANKL (50 ng/ml) (R&D, USA) and M-CSF (30 ng/ml) were added to the culture media and cells were cultured for another 5 days. Tartrate-resistant acid phosphatase (TRAP) staining (Sigma USA) was performed on the 5th day. Antibodies against MMP-9 (Abcam Cambridge, UK) immunofluorescence staining was performed according to the aforementioned method. The supernatant was extracted for ELISA and the BMMs were collected in the lower chamber for RT-qPCR to detect the expression of osteoclast-related genes, including MMP-9, C-FOS, NFATc1. Actin was used as an internal reference, and the primer sequences were designed by Genewiz, as shown in Table 1. Each experiment was repeated three times with three parallel samples (n = 3).

2.11. Establishment of an osteoporosis model and screw placement

Female Sprague-Dawley (SD) rats were provided by the Experimental Animal Center of Soochow University. Animal breeding and related operations were supervised and approved by the Ethics Committee of the First Affiliated Hospital of Soochow University. This study used 3-month-old female SD rats (250–300 g). These rats were placed in a temperature-controlled environment; the temperature was kept at 25 °C, the humidity was kept at 55%, and an alternating 12 h light/dark cycle was utilized. All operations were performed using anesthesia by intraperitoneal injection of 10% (wt.%) chloral hydrate.

Briefly, 6 SD rats were randomly selected from the 86 SD rats for SHAM operation (removal of adipose tissue around the ovaries) and the remained 80 rats for OVX operation (removal of bilateral ovariectomies to induce osteoporosis). Eight weeks later, 6 rats were randomly selected from the OVX group and the 6 rats in the Sham group were sacrificed together. After sample collection, the micro computed tomography (Micro-CT) analysis, hematoxylin-eosin staining (HE) and Masson staining were performed to confirm the establishment of an animal model of osteoporosis (n = 5 samples per group). The remained 72 SD rats in the OVX group were randomly divided into 8 groups with 9 rats in each group: The control group (4 weeks after Screw placement), A-H group (4 weeks after Screw placement), A-H + AB group (4 weeks after Screw placement), A-H + AB-O group (4 weeks after Screw placement) and Control group (8 weeks after Screw placement), A-H group (8 weeks after Screw placement), A-H + AB group (8 weeks after Screw placement), A-H + AB group (8 weeks after Screw placement), A-H + AB-O group (8 weeks after Screw placement). Each SD rat got bilateral experimental with two screws in the distal femora under sterile conditions. 4 weeks and 8 weeks' post-implantation, the rats were sacrificed, respectively. The following investigations, CT analysis (n = 4 samples per group), pull-out test (n = 3 samples per group), toluidine blue hard tissue sections (n = 4 samples per group), HE, Masson staining (n = 3 samples per group) were performed in each group.

Before screw placement, the surgical site was shaved and disinfected. The animal was fixed laterally. By the aseptic surgical techniques, incisions were made in the skin, fascia and periosteum to expose the lateral condyles of the distal femur. First, a 1 mm Kirschner wire was used to drill a medullary canal on the femoral condyle. The hydrogel was injected into the screw channel, and the channel was exposed to ultraviolet irradiation. Finally, an unmodified titanium alloy cortical bone tapping screw (1.5*6 mm, BIOVET, Suzhou, China) was placed *in situ*. After the surgery, each rat was intraperitoneally injected with 80,000 units of penicillin, and the rats were checked every three days.

2.12. Micro-CT

A micro-CT scanning system was used (BRUKER, Kontich, Belgium). The multilevel threshold method (bone threshold = 135; implant threshold = 255) was used to distinguish bone from other tissues. The volume of interest (VOI) in the OVX rats was determined to be 1 mm from the growth plate and 3 mm from the trabeculae of the femoral condyle. In 3D VOI, the BV to TV was calculated as BV/TV. The average absolute values for Tb.N, Tb.Th, Tb.Sp and BMD were determined. The Conn.D was used to characterize the connectivity of the trabecular network. Scanning and reconstruction were performed, and the supporting analysis software was used to rebuild a 3D digital image for each specimen. (n = 5 samples per group).

2.13. Pull-out test

Femur tissues from the rats were fixed at the testing machine (Shanghai Hengyi Precision Instruments Co, China) applied with a 500 N pull force. Briefly, a vascular clamp was used to adequately link the screw heads to the testing machine's jack, and a clamping system drilled with a 5 mm hole was mounted to stabilize the femur tissues. When the

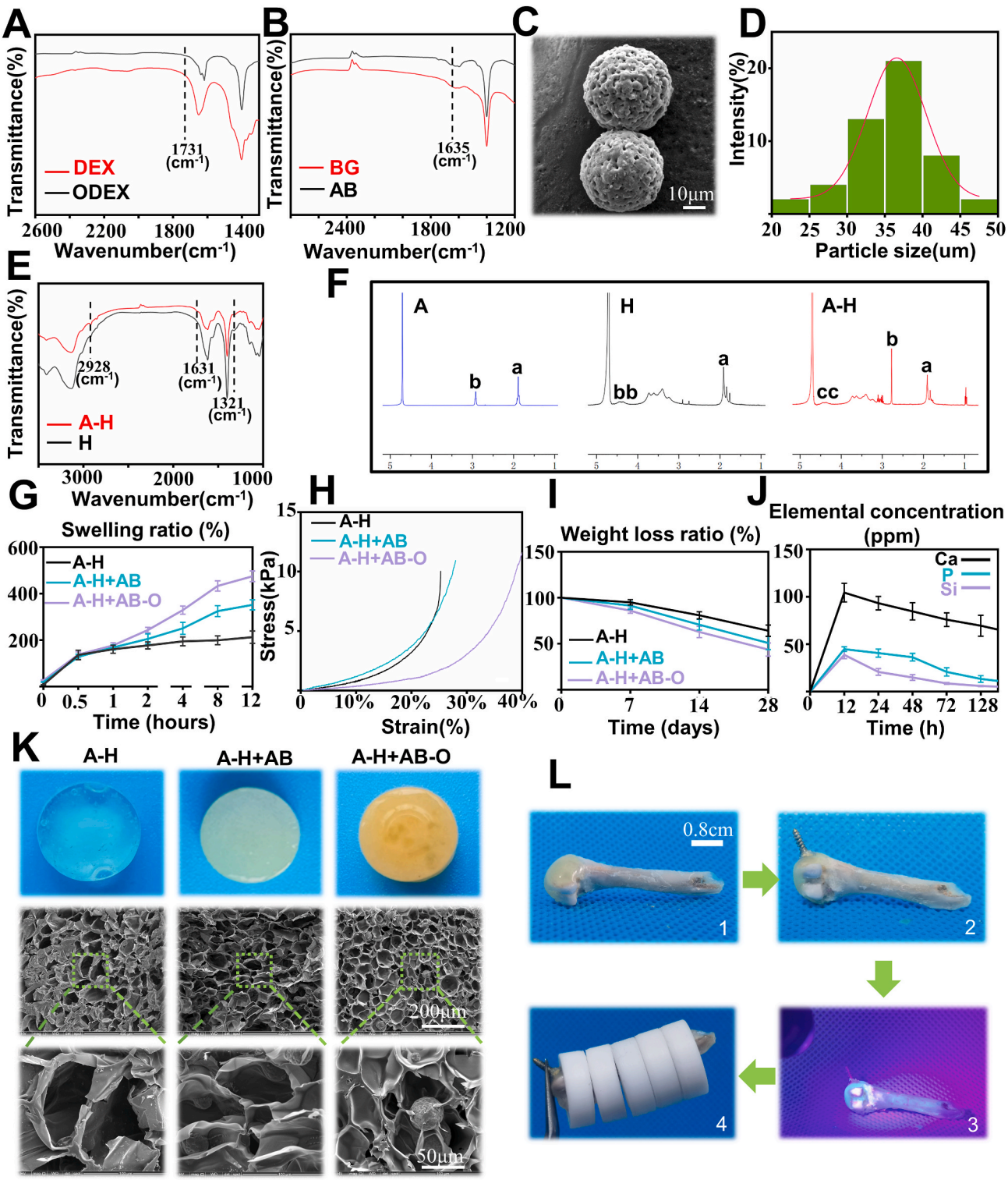

Fig. 1. Physical characterization of the double adhesive hydrogel. A-B) FTIR spectra of DEX, ODEX, BG and AB; C) SEM images of AB; D) Particle size analysis of AB; E) FTIR spectra of H and A-H; F) 1H NMR of A, H, and A-H; G-I) Swelling test, mechanical test, and weight loss analysis of A-H, A-H + AB, and A-H + AB-O (n = 3); J) ions release behavior of the A-H + AB-O hydrogels (n = 3); K) interior SEM images of A-H,A-H + AB,A-H + AB-O; L) digital images of adhesion between the hydrogel and rat's femur (Plastic ring was 1.01 g, rat's femur was 0.83 g).

screw was completely separated from the bone, and the maximum breaking load was recorded, the mechanical test was stopped. (n = 3 samples per group).

2.14. Histology

After the specimens were processed, 200 μ m sections were cut from the tissues with a German EXAKT300CP hard tissue microtome, and the sections were ground to 25 μ m with a German EXAKT400S grinder. Finally, they were polished with 4000 grit sandpaper, and the ground

was stained with methylene blue. (n = 4 samples per group). After removing the screws, they were embedded in paraffin, and the middle part of the defected area was cut longitudinally and processed with H&E and Masson. Image J software was used to quantitively analyze the collagen area ratio around the screws to the total area. (n = 3 samples per group). The expression of collagen type I, OPN, TRAP, and CD31 around the screws was assessed by immunohistochemistry. Image J was used to analyze the positive staining area around the screws. (n = 3 samples per group).

2.15. Statistical analysis

The number of samples (n) used for each experiment was indicated in the figure legends. All data were expressed as mean ± standard deviation (SD). Statistical analyses were performed by GraphPad Prism 7.0 Software (USA). The student's t-test was conducted for analysis of data when comparing two groups. One-way ANOVA or two-way ANOVA followed by Tukey's multiple comparison test was conducted for analysis of data when comparing multiple groups. Difference with a probability value (p) < 0.05 were considered to be statistically significant. All experiments were performed with at least three independent samples.

3. Results and discussion

3.1. Synthesis and physical properties of the double-bonded hydrogels

The A-H + AB-O double-adhesive hydrogel consisted of oxidized dextran-modified aminated bioactive glass (AB-O) and alendronate grafted methacryloyl hyaluronic (A-H). After the oxidation of dextran, the Fourier transform infrared spectroscopy (FTIR) curve exhibited a peak at 1731 cm^{-1} which indicated that a large number of aldehyde groups were successfully grafted on the dextran molecular chain through the oxidation reaction (Fig. 1A) [30]. The APTES modified BG (Fig. 1B) was also proved to contain many grafted amino groups on its surface, and a peak representing NH_2 was found at 1635 cm^{-1} [31]. Scanning electron microscopy (SEM) (Fig. 1C) indicated that the aminated 45S5 BG surface was smooth, and the particle size was homogeneous. The average diameter of the AB was 35.52 ± 5.51 μm (Fig. 1D). The oxidized dextran was bound to the aminated bioactive glass through an amide bond. The additional aldehyde group on the oxidized dextran molecular chain can combine with the amino group of bone tissue collagen, mediating the double-bonding hydrogel capacity that results in organic adhesion and bone formation. According to the previous literature [27], the carboxyl group is activated by NHS and EDC, and the amino group on alendronate sodium and the carboxyl group on methacryloyl hyaluronic acid react with each other to produce methacryloyl hyaluronic acid grafts with alendronate (A-H). The FTIR curve showed

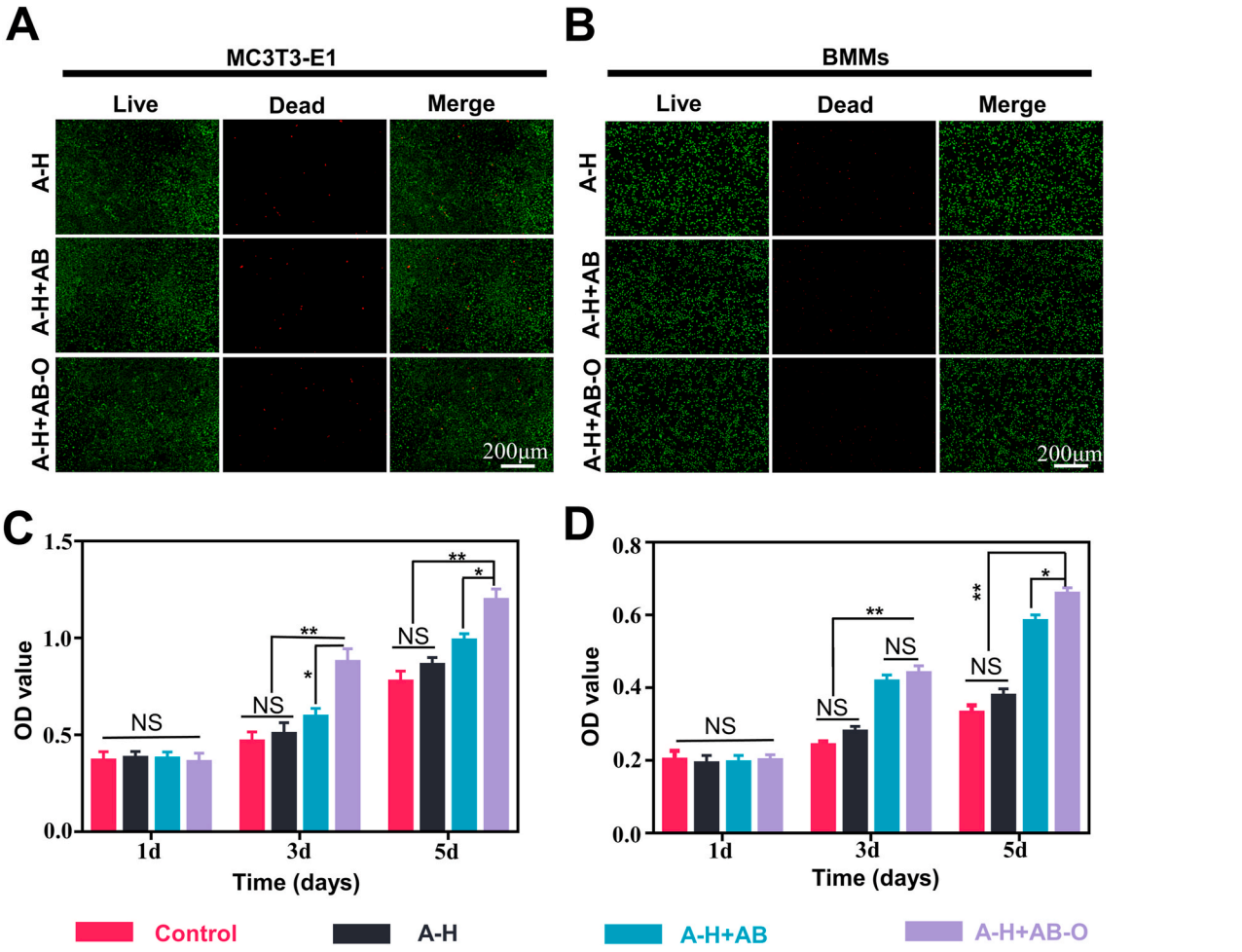

Fig. 2. Evaluation of the biocompatibility of the organic-inorganic, double-bonded hydrogels *in vitro*. A-B) Live/dead staining of BMMs and MC3T3-E1 cells on different hydrogels after 3 days' co-culture. C-D) CCK-8 assay of BMMs and MC3T3-E1 cells. (n = 3, all values were mean ± std. dev., NS, not significant, *p < 0.05, **p < 0.01 when comparing A-H + AB-O and other groups via two-way ANOVA analysis followed by Tukey's multiple comparison test by GraphPad Prism 7.0 Software (USA)).

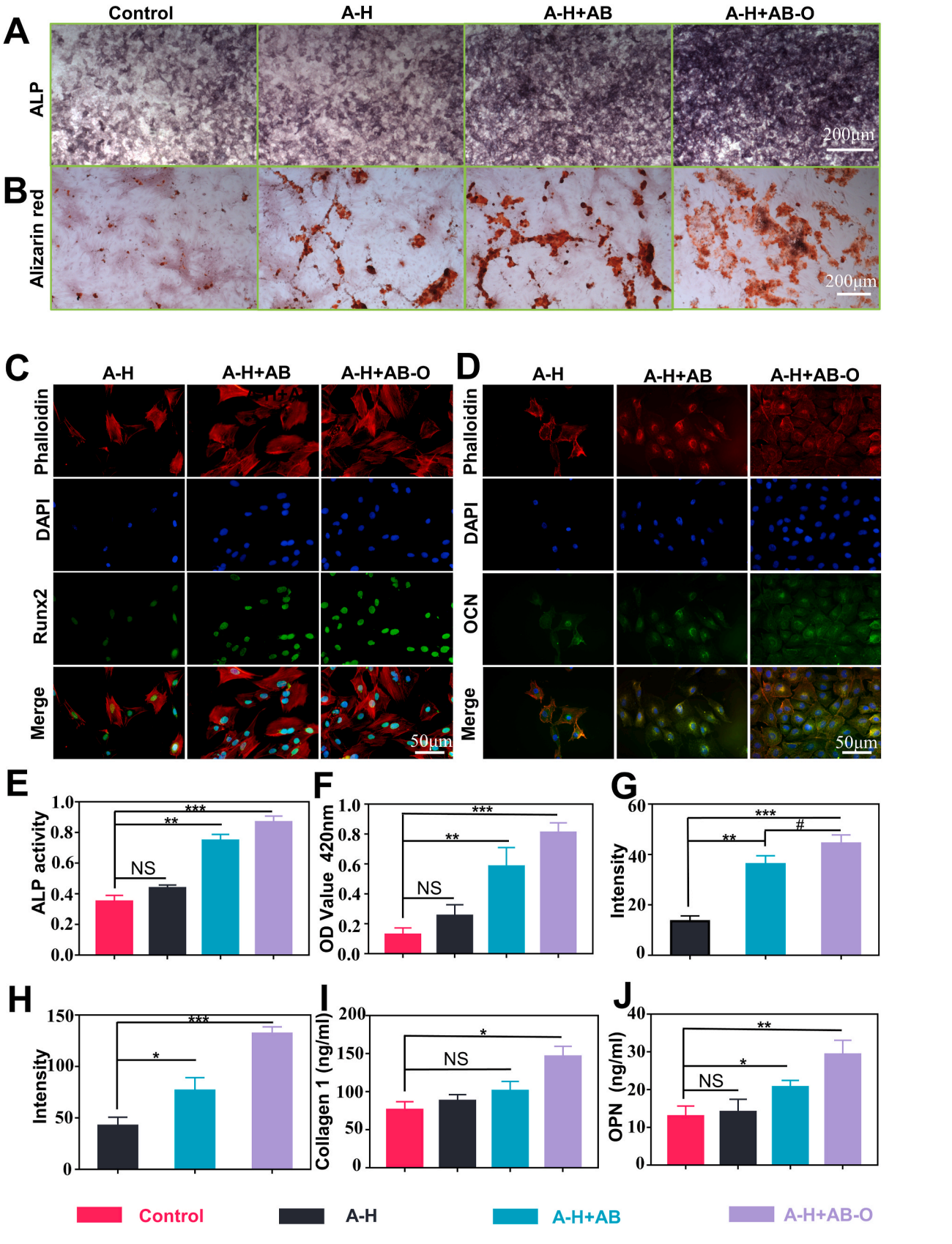

(caption on next page)

Fig. 3. Osteogenesis evaluation. A-B) ALP and alizarin red staining of MC3T3-E1 cells cultured in osteogenic medium with different hydrogel groups. C-D) immunofluorescence staining of RUNX2 on day 7 and OCN on day 14, with the nuclei stained blue (DAPI), the proteins stained green and the cytoskeletal structure stained red. E-F) quantitative analysis of ALP activity and alizarin red staining results (n = 3, all values were mean ± std. dev., NS, not significant, **p < 0.01, ***p < 0.001 when comparing Control and other groups via one-way ANOVA analysis followed by Tukey's multiple comparison test by GraphPad Prism 7.0 Software (USA)). G-H) semiquantitative analysis of the fluorescence intensity of RUNX2 and OCN (n = 3, all values were mean ± std. dev., NS, not significant, *p < 0.05, **p < 0.01, ***p < 0.001 when comparing A-H and other groups; #p < 0.05 when comparing A-H + AB and A-H + AB-O via one-way ANOVA analysis followed by Tukey's multiple comparison test by GraphPad Prism 7.0 Software (USA)). I-J) ELISA results of the concentration of collagen I and OPN in the cell supernatant (n = 3, all values were mean ± std. dev., NS, not significant, *p < 0.05, **p < 0.01 when comparing Control and other groups via one-way ANOVA analysis followed by Tukey's multiple comparison test by GraphPad Prism 7.0 Software (USA)). (For interpretation of the references to colour in this figure legend, the reader is referred to the Web version of this article.)

that a new peak at 2928 cm^{-1}, which is attributed to the vibration of the imino group (-CH2-) as the A containing an imino group was successfully grafted onto H. Moreover, the wave peak at 1631 cm^{-1} is slightly widened, due to the formation of amide bonds. The peak at 1321 cm^{-1} is weaker, suggesting the consumption of carboxyl groups after A grafting (Fig. 1E). The 1H NMR spectra also confirmed the successful synthesis of A-H. Two characteristic peaks (Fig. 1F) appear at 2.95 ppm and 1.92 ppm in A. The peaks at 1.9 ppm and 3.12–4.51 ppm are attributed to the methyl proton and ring of the acetamido group in H, respectively. The peak corresponding to the amide bond appears at 2.70 ppm in A-H, confirming the successful bonding of A to H [32]. H grafted with A can be combined with calcium in the hydroxyapatite of bone tissue, also favoring the double-bonding capacity of the hydrogel, inorganic adhesion and inhibiting bone resorption.

The swelling capacity is an important parameter of hydrogels. Here, the swelling ratio at different time point was calculated to determine the water absorption capacity of the hydrogels. As shown in Fig. 1G, after 12 h, the swelling ratio of A-H + AB-O group, A-H + AB group and A-H group was 482.9%, 337%, and 184.9%, respectively. Compared to the other two groups, the water absorption capacity of the A-H + AB-O group was greater by 145.9% and 298%, respectively. This might be related to the fact that the binding tightness of the long-chain hydrogel molecules decreased with the addition of AB and O, leading to the higher swelling ratio. This capacity indicated that the hydrogel could fill the loose and porous structure of osteoporotic areas in the presence of body fluids.

To investigate the mechanical properties of the hydrogel after the addition of AB and O, a mechanical test was performed (Fig. S1) [33]. Fig. 1H showed that, with the increased strain ratio, the A-H + AB-O group exhibited a smaller elastic modulus than the other two groups demonstrating that the composite hydrogel had good ductility and toughness, which may be attributed to the loose cohesion of hydrogel molecules.

To further explore the structural stability of the hybrid hydrogel, we conducted a weight loss experiment [31]. The results presented in Fig. 1I illustrated that after the hydrogels were immersed in PBS for 7 days, there was no difference in the weight loss ratio among all the three groups. ($p > 0.05$, $n = 3$) By the 28th day, the weight loss ratio of A-H + AB-O reached 43.5%, which was not significantly different from that of the other two groups indicating a long degradation time of the A-H + AB-O group.

The ions release behaviors of A-H + AB-O hydrogels in simulated body fluid (SBF) were presented in Fig. 1J. Due to the rapid exchange of Ca^{2+} in the BG with H+ in the solution, the release of Ca^{2+} increased rapidly within 24 h. This ion exchange formed silanol groups (Si–OH) on the surface of the bioactive glass and increased the pH of the solution. A high pH will damage the silicate network and cause the release of Si^{2+}. The silicon-rich layer formed on the bioactive glass surface adsorbed Si^{2+} and phosphate ions in the solution, leading to the gradually decreasing concentration of Si^{2+} and P^{3+} in the solution [34].

The SEM results (Fig. 1K) revealed that each hydrogel group had a sponge-like structure with uniform porosity and good interconnectivity. The microstructure analysis of the A-H + AB-O hydrogel showed that this hydrogel exhibited a 3D composite pore structure with a rough surface. The pore distribution was uniform and interpenetrated with a diameter of 100 ± 20 μ m. Besides, the BG particles were homogeneously integrated into these pores. Overall, the organic-inorganic, double-adhesive hydrogel demonstrated a good microphysical structure with even distribution of biologically active microspheres inside the pores.

The adhesion between hydrogels and the surface of bone tissues is a critical factor in promoting the repair and regeneration of cancellous bone [35]. The adhesion ability between the hydrogel and bone tissues was evaluated *in vitro* (Fig. 1L). In brief, the A-H + AB-O hydrogel was injected onto the femoral condyle of rat *in vitro* (Fig. 1L–1), then the screw cap was embedded in the A-H + AB-O (Fig. 1L–2). After UV irradiation, the screw was firmly fixed on the surface of the femoral condyle by the solidified hydrogel (Fig. 1L–3). Additional weight (total weight: 5.88 g) was added to the femur. Then tweezer was used to hold the screw on the femur, the whole system was still stable (Fig. 1L–4). In spite of the absence of chemical bonding between the screw and the hydrogel, this phenomenon in Fig. 1L–4 could be attributed to the adhesiveness between the hydrogel and bone as well as the stiffness of the hydrogel which embedding the screw.

3.2. Evaluating the biocompatibility of the double-bonded hydrogels

To evaluate the biocompatibility of the double-bonded hydrogels, the Live/Dead staining was performed on BMMs and MC3T3-E1 cells *in vitro*. Limited dead cells in the A-H + AB-O hydrogels confirmed the good biocompatibility of A-H + AB-O hydrogels compared to the other two groups (Fig. 2A and B). To quantitatively analyze cell proliferation in the different groups, CCK-8 assays were performed (Fig. 2C and D). After one day of co-cultivation, the optical density (OD) values for each group were not statistically different ($p > 0.05$, $n = 3$). After 5 days, the OD values for the A-H + AB-O group were higher than that of two other groups, and the differences were statistically significant ($p < 0.05$, $n = 3$). SEM images of the hydrogel cultured with MC3T3-E1 cells showed that the cells adhered to the surface of hydrogel with stretched morphology. In addition, a large number of cell colonies grow in clusters on the hydrogel surface. The neighboring cells formed a stretched mesh structure (Fig. S2). These results indicated that the hybrid hydrogel was biocompatible.

3.3. In vitro osteogenesis evaluation

Alkaline phosphatase (ALP) is one of the essential proteases involved in the osteogenic differentiation process. ALP can hydrolyze organic phosphates, increase the local PO_4^{3-} concentration, and promote calcium salt deposition after combining with Ca^{2+}. Calcified nodules are an important manifestation of matrix mineralization [36]. To verify the osteogenic ability of the hydrogels *in vitro*, ALP staining, and the alizarin red staining were respectively performed on MC3T3-E1 cells cultured on the surface of different hydrogels on days 7 and 21. The results of the ALP staining revealed that the dyed extent of the A-H + AB-O group and the A-H + AB group was significantly higher than those of the A-H group and the control group due to the additional BG (Fig. 3A). As shown in Fig. 3B, for the alizarin red staining, a small number of red mineralized nodules with irregular shapes and small clumps were observed in the control group and the A-H group. However, in the A-H + AB-O and A-H

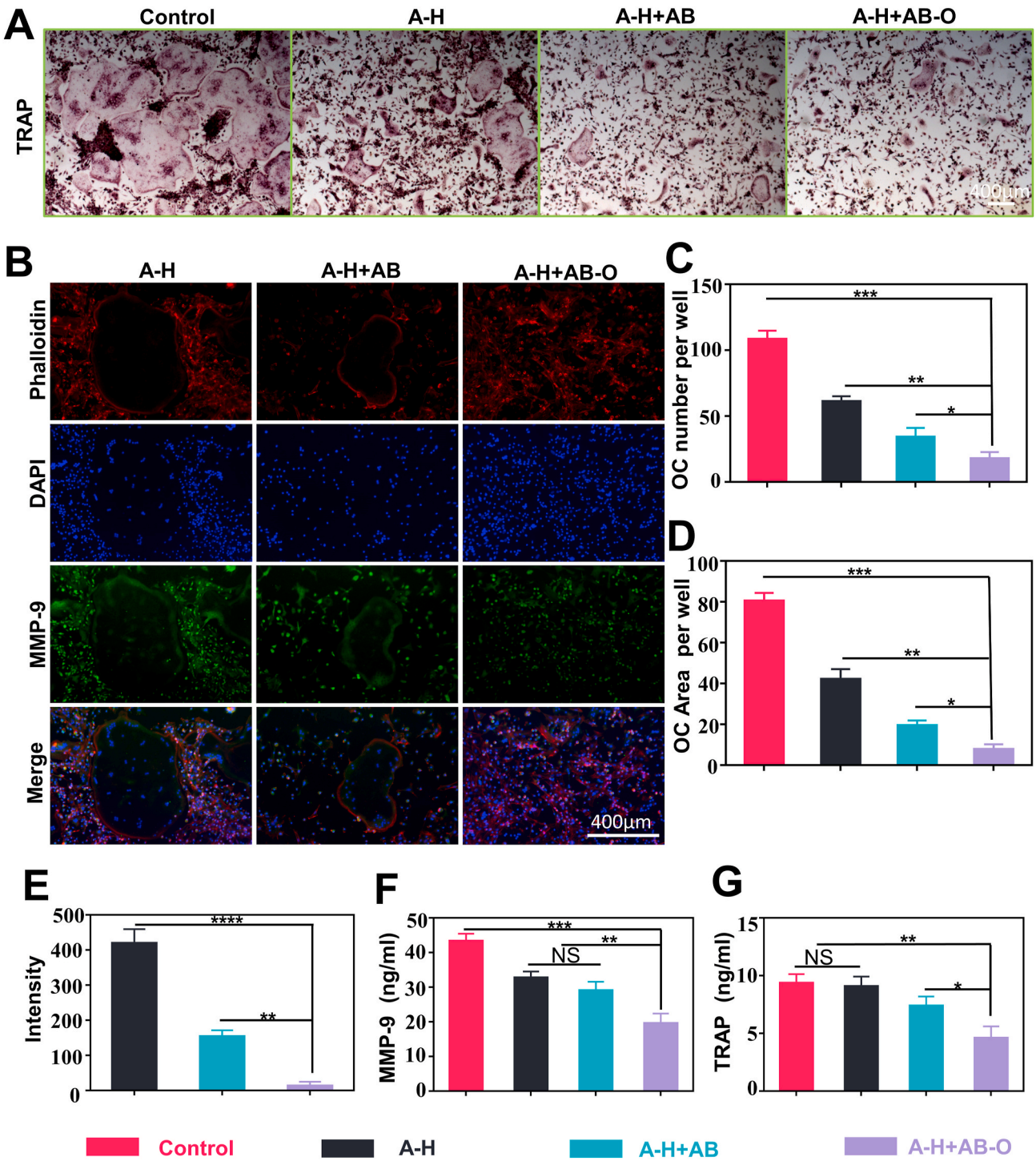

Fig. 4. Osteoclast evaluation. A) TRAP staining of BMMs cells cultured in RANKL-containing medium with different hydrogel groups. B) Immunofluorescence assays for MMP-9 on day 5, with the nuclei stained blue (DAPI), the protein stained green and the cytoskeletal structure stained red. C-D) quantitative analysis of TRAP positive cell number; Quantitative analysis of TRAP positive staining area. E) semiquantitative analysis of the fluorescence intensity in MMP-9. F-G) ELISA analysis of the concentration of MMP-9 and TRAP concentrations on day 5 in the cell supernatant. (n = 3, all values were mean ± std. dev., NS, not significant, *p < 0.05, **p < 0.01, ***p < 0.001 when comparing A-H + AB-O and other groups via one-way ANOVA analysis followed by Tukey's multiple comparison test by GraphPad Prism 7.0 Software (USA)). (For interpretation of the references to colour in this figure legend, the reader is referred to the Web version of this article.)

+ AB groups, many red mineralized nodules were observed. Some of these nodules were clumps with brown or red staining, indicating strong positive reactions. In this study, the positive level of ALP staining and the ALP activity in the A-H + AB-O group was higher than that in the other groups, especially the control group on the 7 days ($p < 0.001$, $n = 3$) (Fig. 3E). After dissolving the mineralized nodules with perchloric acid, we measured the absorbance of the dissolving solution at 420 nm, as shown in Fig. 3F. The mineralization level in the A-H + AB-O group and the A-H + AB group were both significantly higher than that in the control group and the A-H group, and there was no significant difference between the A-H + AB-O group and the A-H + AB group ($p > 0.05$, $n = 3$). Since the RUNX2, OCN and OPN were the gene markers of

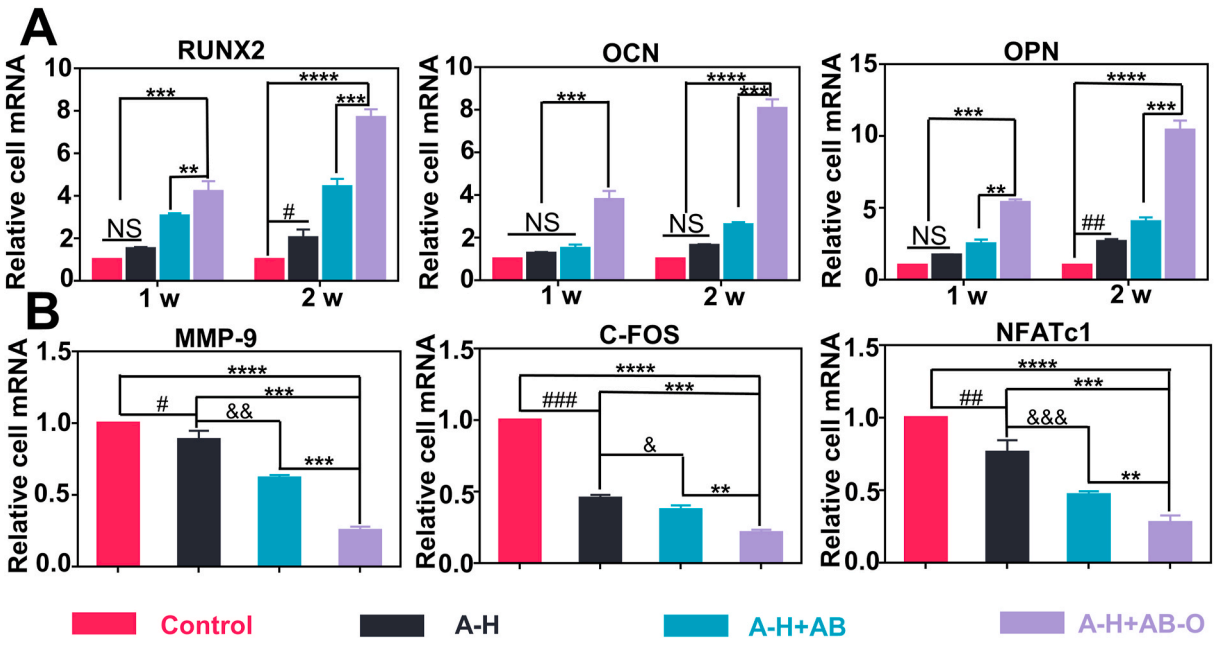

Fig. 5. A) Expression level of osteogenesis-related genes including RUNX2, OCN, OPN (n = 3, all values were mean ± std. dev., NS, not significant, $^{**}p < 0.01$, $^{***}p < 0.001$, $^{****}p < 0.0001$ when comparing A-H + AB-O and other groups; $^{\#}p < 0.05$, $^{\#\#}p < 0.01$ when comparing Control and A-H via two-way ANOVA analysis followed by Tukey's multiple comparison test by GraphPad Prism 7.0 Software (USA)). B) Expression level of osteoclastogenesis-related genes including MMP-9, c-FOS, NFATc1 on day 5 (n = 3, all values were mean ± std. dev., NS, not significant, $^{**}p < 0.01$, $^{***}p < 0.001$, $^{****}p < 0.0001$ when comparing A-H + AB-O and other groups; $^{\#}p < 0.05$, $^{\#\#}p < 0.01$, $^{\#\#\#}p < 0.001$ when comparing Control and A-H; $^{\&}p < 0.05$, $^{\&\&}p < 0.01$, $^{\&\&\&}p < 0.01$ when comparing A-H and A-H + AB via one-way ANOVA analysis followed by Tukey's multiple comparison test by GraphPad Prism 7.0 Software (USA)).

osteogenesis [37], we performed RUNX2 and OCN immunofluorescence staining (Fig. 3C and D). The results showed that the fluorescence level of RUNX2 and OCN in the A-H + AB-O group was significantly more potent than that in the A-H and A-H + AB groups, which was consistent with the results of semi-quantitative fluorescence analysis (Fig. 3G and H). We also examined two osteogenic indicators COL-1 (7 days) and OPN (14 days) in the culture supernatant (Fig. 3I and J). The expression of the two osteogenic indicators in the supernatant of the A-H + AB-O group was higher than that in the supernatant of the control group ($p < 0.05$, $n = 3$). RT-qPCR was performed to evaluate the expression levels of osteogenic genes (RUNX2 , OCN, OPN) expression at 7 and 14 days (Fig. 5). The results of RT-qPCR were consistent with the results of osteogenic indicators in the culture supernatants and confirmed the aforementioned results.

3.4. *In vitro osteoclast evaluation*

Tartrate resistant acid phosphatase (TRAP) is highly expressed in osteoclasts. The hydrogels and BMMs were co-cultured in a transwell for 5 days and then stained with TRAP. TRAP staining results (Fig. 4A) showed that the alendronate-loaded group significantly inhibited RANKL-induced osteoclast differentiation. The quantitative analysis of the staining results (Fig. 4C) indicated that the number of osteoclasts decreased from 61.1 ± 3.3 (A-H) to 17.7 ± 4.1 (A-H + AB-O), and the positive staining area of osteoclasts (Fig. 4D) decreased from 42 ± 4.08% (A-H) to 7.7 ± 2.1% (A-H + AB-O), which may be attributed to the high local concentration of alendronate released from the A-H + AB-O group. Compared to the pure A-H group, the A-H + AB-O group exhibited reduced fluorescence in the osteoclast-related protein, MMP-9 (Fig. 4B). The semi-quantitative fluorescence intensity decreased from 419.2 ± 32.7 (A-H group) to 13.08 ± 9.45 (A-H + AB-O group) (Fig. 4E). We also examined the osteoclast indexes, MMP-9 and TRAP, on day 5 in the culture supernatant (Fig. 4F and G). The expression of these two osteoclast indexes in the supernatant of the A-H + AB-O group was lower than that in the supernatant of the other groups. In addition, it was significantly different from the control group ($p < 0.01$, $n = 3$). NFATc1 and C-FOS are downstream genes promoting the differentiation of osteoclast precursor cells into mature osteoclasts in the NF-kB pathway [38]. We also performed RT-qPCR to evaluate the gene expression levels of MMP-9, C-FOS and NFATc1 (Fig. 5). The RT-qPCR results were consistent with the TRAP staining, semi-quantitative fluorescence analysis, and ELISA.

3.5. *Establishing the osteoporosis model in vivo*

According to the previous reports [39], we used SD rats to establish the osteoporosis model through ovariectomy (Fig. 6A). Micro-CT was performed on SHAM group and OVX group after 8 weeks to confirm the establishment of osteoporosis. According to the Micro-CT results, the bone mass of the femoral condylar was decreased, the trabecular bone structure was disordered, and the bone marrow cavity was enlarged in the OVX group compared to the SHAM group (Fig. 6B). In addition, H&E and Masson staining (Fig. 6C and D) also indicated the differences between the two groups. Specially, the normal plate-shaped trabecular bone was observed in the SHAM group. In contrast, rod-shaped trabecular bone degeneration was observed in the OVX rats. Micro-CT quantitative analysis (Fig. 6E, F, G, H, I) further revealed that bone mineral density (BMD), the bone volume (BV), connectivity density (Conn. D), number of trabecular bones (Tb. N) and trabecular bone thickness (Tb. Th) in the region of interest were reduced by 74%,69%, 29% and 57% in the OVX group, respectively. The trabecular bone spacing (Tb. Sp) correspondingly increased by a factor of 6.8 after 8 weeks post ovariectomy (Fig. 6J). These results confirmed the successful establishment of the osteoporosis rat model.

3.6. *In vivo application of the double-bonded hydrogel*

Eight weeks after the ovariectomy, titanium (Ti) screws were placed in all osteoporotic rats with femoral condyles (Fig. 7A). In this study, the control group was denoted as the PBS group. The A-H, A-H + AB, and A-

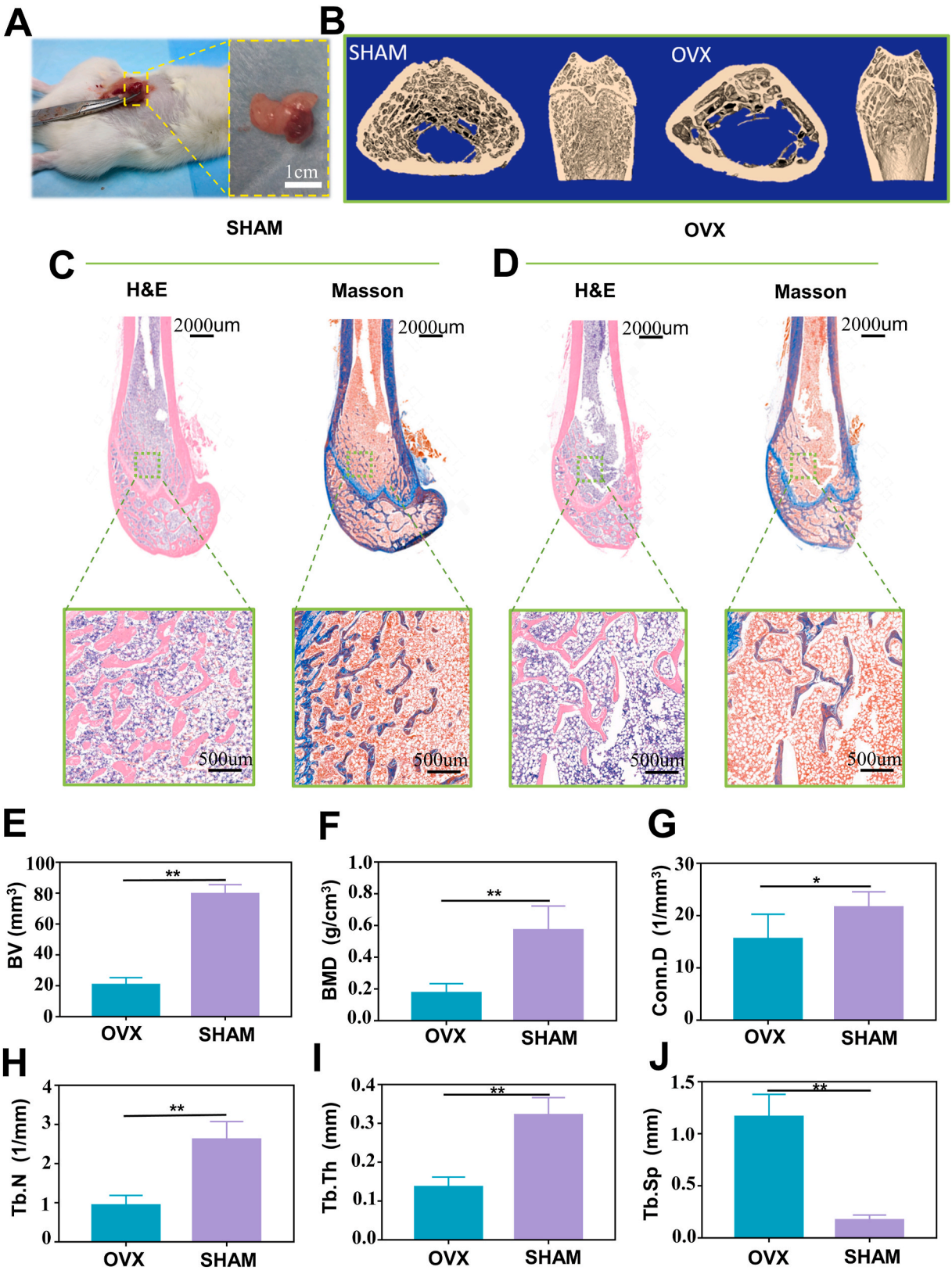

Fig. 6. Establishment of the animal model. A) Ovariectomy image of SD rats. B) Micro-CT 3D reconstructed images. C-D) H&E and Masson's trichrome staining. E-J) quantitative analysis of Micro-CT results including BV, BMD, Conn.D, Tb.N, Tb.Th, and Tb.Sp (n = 5, all values were mean ± std. dev., *p < 0.05, **p < 0.01 when comparing OVX and SHAM via student's t-test analysis by GraphPad Prism 7.0 Software (USA)).

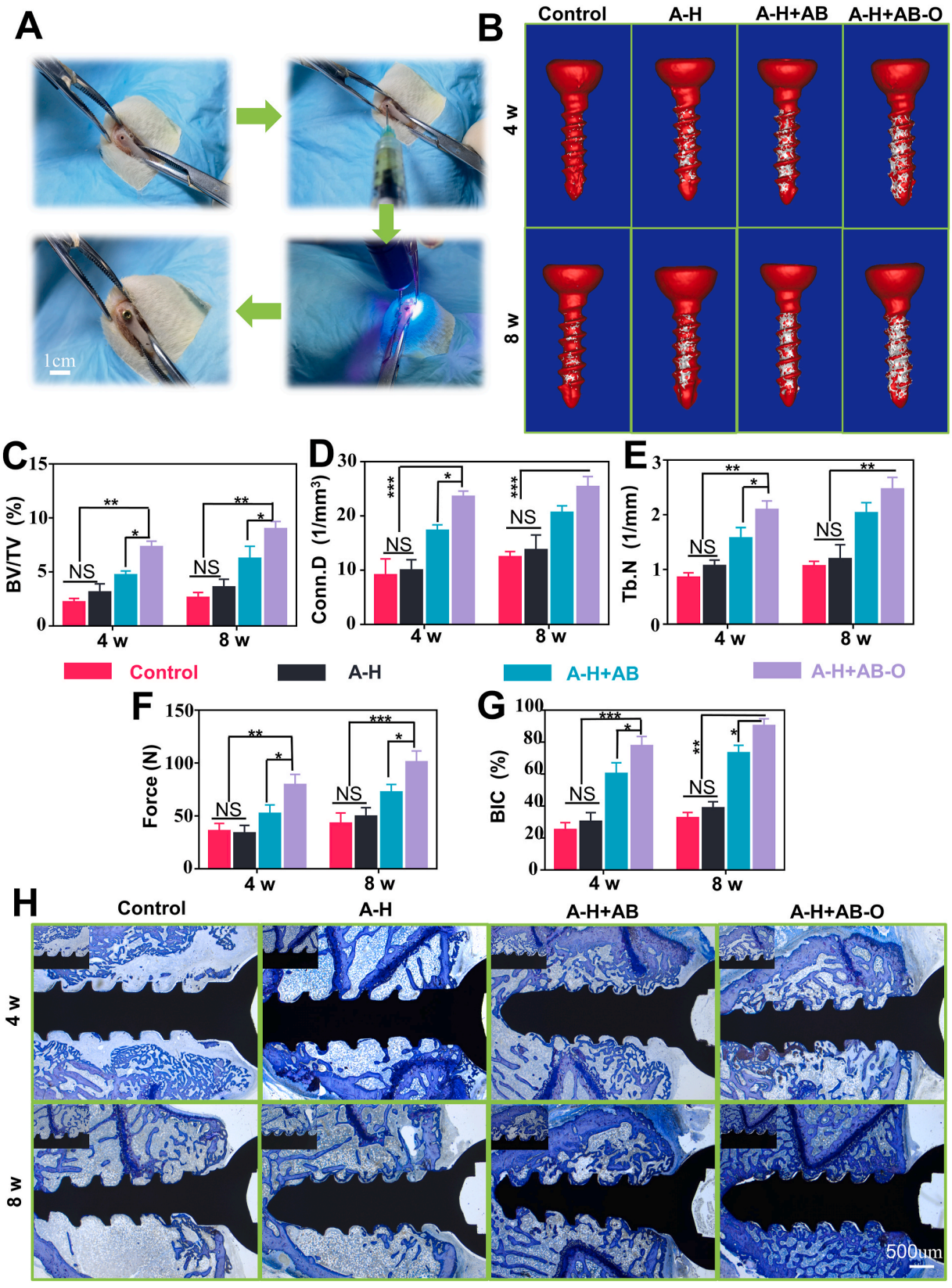

Fig. 7. In vivo application of the double-bonded hydrogel. A) The process of screw implantation in SD rats. B) Micro-CT 3D reconstructed images. C-E) Micro-CT analysis of BV/TV, Conn.D and Tb.N (n = 4, all values were mean ± std. dev., NS, not significant, *p < 0.05, **p < 0.01, ***p < 0.001 when comparing A-H + AB-O and other groups via two-way ANOVA analysis followed by Tukey's multiple comparison test by GraphPad Prism 7.0 Software (USA)). F) The results of pull-out testing (n = 3, all values were mean ± std. dev., NS, not significant, *p < 0.05, **p < 0.01, ***p < 0.001 when comparing A-H + AB-O and other groups via two-way ANOVA analysis followed by Tukey's multiple comparison test by GraphPad Prism 7.0 Software (USA)). G) Histomorphometric results of BIC (n = 4, all values were mean ± std. dev., NS, not significant, *p < 0.05, **p < 0.01, ***p < 0.001 when comparing A-H + AB-O and other groups via two-way ANOVA analysis followed by Tukey's multiple comparison test by GraphPad Prism 7.0 Software (USA)). H) Representative samples stained with toluidine.

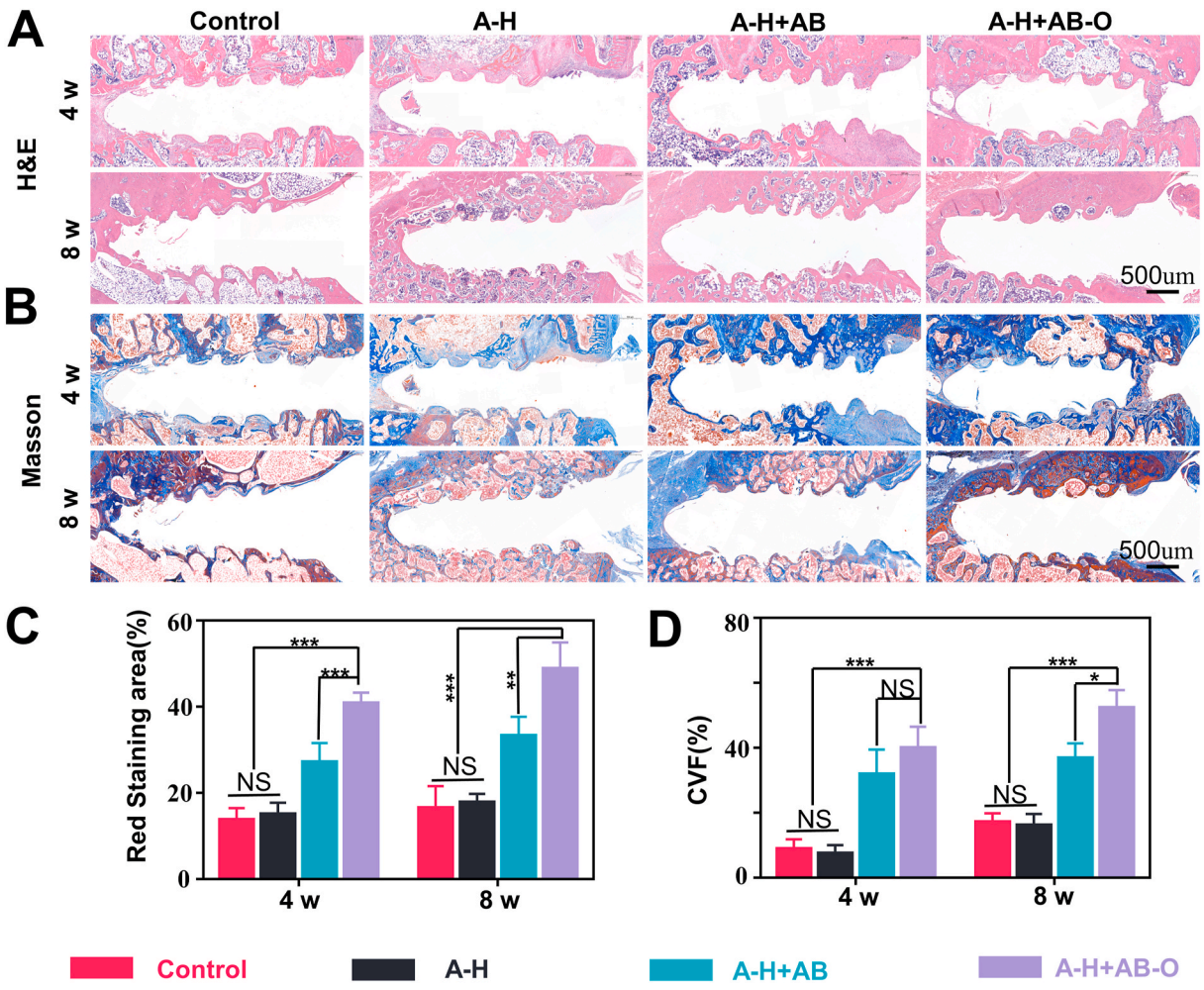

Fig. 8. H&E and Masson staining. A-B) H&E and Masson staining in each group, 4- and 8- weeks post-surgery. C-D) quantitative results of H&E and Masson staining in the proportion of bone collagen (n = 3, all values were mean ± std. dev., NS, not significant, *p < 0.05, **p < 0.01, ***p < 0.001 when comparing A-H + AB-O and other groups via two-way ANOVA analysis followed by Tukey's multiple comparison test by GraphPad Prism 7.0 Software (USA)).

H + AB-O hydrogels were respectively injected into the screw channel in femoral condyles before screw implantation, denoted as A-H group, A-H + AB group, and A-H + AB-O group. The screw was fixed precisely on the femoral condyle. The size of the Ti screw was completely matched with the rat femoral condyle. After 4- and 8-weeks' implantation, all rats were sacrificed, and the femoral condyles implanted with Ti screws were analyzed by Micro-CT (Fig. 7B–E). Interface osteogenesis and the formation of the new bone surrounding Ti screws were evaluated in the different hydrogel groups. After 4- and 8-weeks' implantation, the percentage of BV/TV in the A-H + AB-O group was significantly enhanced compared to that in the other groups ($P < 0.05$, $n = 4$). This result might be attributed to the dual organic-inorganic bonding of the A-H + AB-O hydrogel in the screw channel, making the whole system stable regardless of the influence caused by the body fluids leading to the enhanced osseointegration. After eight weeks, the BV/TV in the A-H + AB-O group (8.967 ± 0.709%) increased 2.51- and 1.22- times compared to that in the A-H group (3.567 ± 0.764%) and the A-H + AB group (7.333 ± 0.503%). In addition, the BV/TV in the A-H + AB-O group after eight weeks was higher than that in four weeks (7.300 ± 0.557%). A significant better interface osteogenesis and good bone condition were observed in the A-H + AB-O group, indicating that the organic-inorganic, double-bonding hydrogel could effectively improve the metabolism of disordered bone around the implants. For example, after 8 weeks, the Conn. D and Tb. N of the A-H + AB-O group (25.337 ± 1.932%, 2.464 ± 0.219%) was significantly higher than that of the control group (12.403 ± 1.046%, 1.059 ± 0.090%) ($P < 0.01$, $n = 4$). The BV in the A-H group and the A-H + AB group also slightly improved. However, hydrogel in these two groups only exhibited single functions (either improved adhesion or induced osteogenesis), but the A-H + AB-O group had improved adhesion and induced osteogenesis capabilities simultaneously. These results confirmed that the key factors, such as organic-inorganic double bonding, osteogenesis promotion, and osteoclast inhibition, were equally important in promoting the reconstruction of cancellous bone around the implants and enhancing newly formed bone condition, especially in the osteoporosis model. The anchorage force of the screws was measured by pull-out testing (Fig. 7F, Fig. S3. S4) [21]. After 8 weeks, the pull-out force for the screws in the A-H + AB-O group was 2.35 times higher than that in the control group and 1.27 times higher than the pull-out force for the screws in the A-H + AB-O group after four weeks. The trend was consistent with the formation of new bone around the implanted screw.

3.7. Quantitative histology analysis and tissue morphology

In this study, toluidine blue staining was used to observe bone growth in the threaded area of the bone/screw interface and the implant-bone contact (BIC) in osteoporotic rats [40]. As shown in Fig. 7H, after 4- and 8- weeks post-surgery, there was limited bone formation around the screw in the control group, while the new bone formation in the A-H + AB group, and A-H + AB-O group was enhanced.

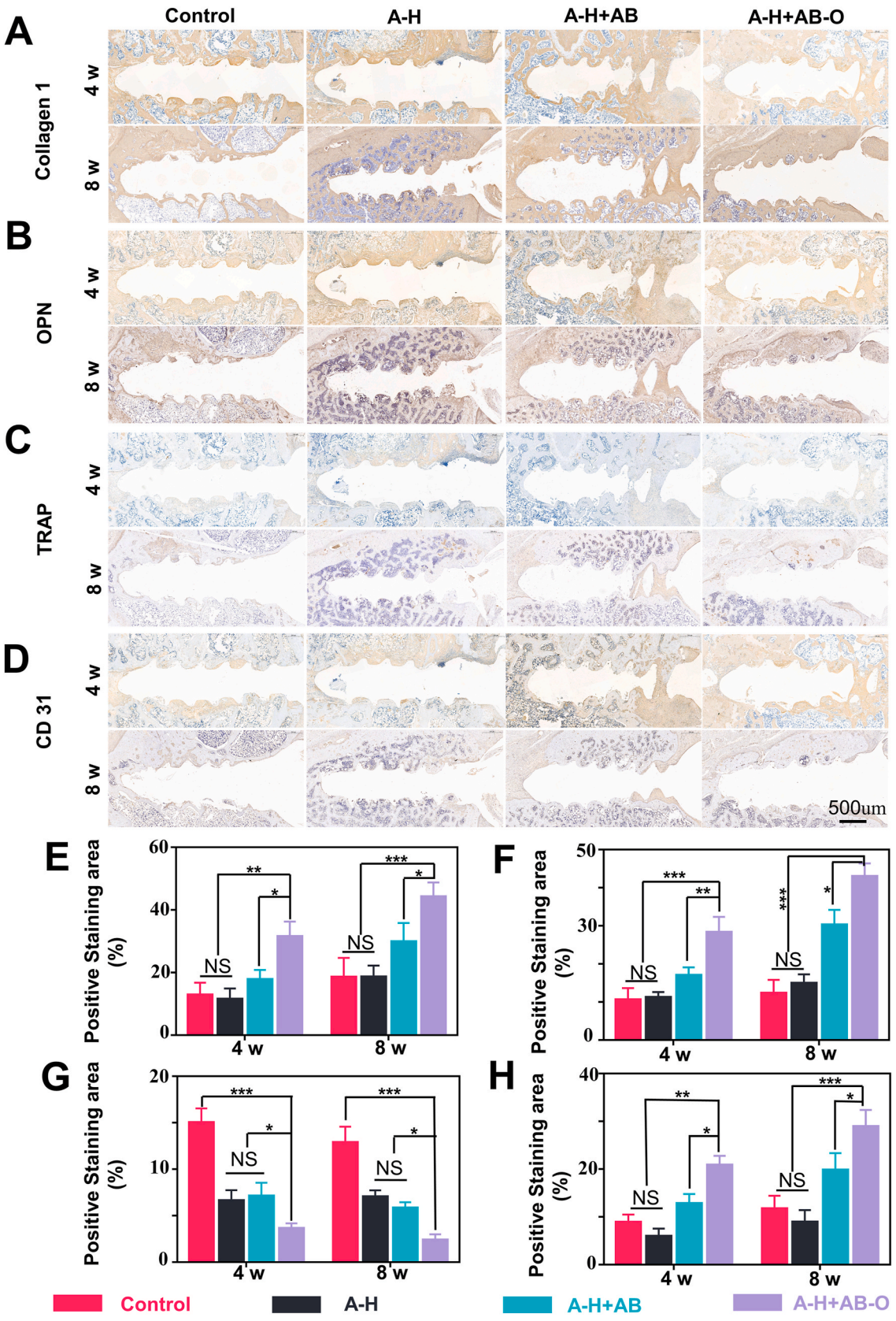

Fig. 9. Immunohistochemistry. A-D) immunohistochemistry of collagen type I, OPN, TRAP, and CD31. E-H) quantitative results in the proportion of positive areas in collagen I, OPN, TRAP, and CD31 (n = 3, all values were mean ± std. dev., NS, not significant, *p < 0.05, **p < 0.01, ***p < 0.001 when comparing A-H + AB-O and other groups via two-way ANOVA analysis followed by Tukey's multiple comparison test by GraphPad Prism 7.0 Software (USA)).

Moreover, the hard tissue slices of the A-H + AB-O group showed an increased continuous bone matrix formation around the screws and a significant increase in the surrounding bone trabeculae. The BIC is one of the standards used to quantify the degree of osseointegration [41,42]. As shown in Fig. 7G, compared with that of the control group after 8 weeks post-surgery, the BIC of A-H + AB group, and A-H + AB-O group increased by 2.25, and 2.77, respectively. The BIC of the A-H + AB-O group after 8 weeks post-operation also increased by 1.16 compared with that of the experimental group after 4 weeks post-operation. From the former results, osteoclast formation was greatly inhibited by alendronate, and bioactive glass exhibited excellent bone-forming ability; these factors greatly promoted the metabolism of bone by balancing osteogenesis and bone resorption. In our study, the enhanced osseointegration around the implants had a tight relationship with the synergistic effects of organic-inorganic double adhesion facilitating cell growth and reducing hydrogel loss in body fluids. Although this hypothesis should be confirmed in future studies, our results revealed that the organic-inorganic, double-bonding hydrogel improved osseointegration and cancellous bone reconstruction around screws under osteoporotic conditions.

To explore the osteogenesis of the hybrid hydrogel in the screw channel, we took cross-sections of the screws removed from the samples after 4- and 8- weeks post-surgery for histological sectioning and quantitative analysis (Fig. 8A–D). After 4 weeks post-operation, the number of red-stained collagen fibers (H&E) and blue-stained collagen fibers (Masson staining) in the A-H + AB and A-H + AB-O groups were greater than that in the control group and the A-H group. Fibrous connective tissue was mostly filled around the nail channel in the control group and the A-H group. The trend was more obvious 8 weeks' post-operation. Further quantitative analysis showed that compared with that of the control group, A-H group, and A-H + AB group after 8 weeks post-operation, the H&E red-stained area in the A-H + AB-O group after 8 weeks post-operation, was higher by 2.96, 2.74, and 1.47, respectively. Compared with that of the A-H + AB-O group after 4 weeks post-operation, the H&E red-stained area in the A-H + AB-O group after 8 weeks post-operation was higher by a factor of 1.2. Similar trends were also observed in the Masson staining.

4- and 8- weeks post-surgery, collagen I and OPN immunohistochemical staining indicated that a wide range of positive staining areas appeared in the tissue surrounding the screw channel (Fig. 9A. B). The expression level of collagen I and OPN were higher in the A-H + AB-O group than in the control group, A-H group, and A-H + AB group. The quantitative analysis results (Fig. 9E and F) were also consistent with this trend. TRAP staining was used to identify the osteoclasts in the histological sections of samples, 4- and 8- weeks post-operation (Fig. 9C). As expected, the control group showed a larger trap-positive area than that in the other groups due to the excessive osteoclastic activity during osteoporosis. However, few osteoclasts around the screw channel in the A-H + AB-O group attributed to the organic adhesion of the double-bonding hydrogel on the cancellous bone, leading to the local release of alendronate sodium with high concentration. The quantitative results of the TRAP staining were consistent with this trend (Fig. 9G). Bioactive glass can release silicon ions that can enhance the hydrogel's ability in promoting vascularization and tissue regeneration [43]. CD31 is known as a member of the immunoglobulin superfamily. It mediates cell adhesion through endothelial cell expression [44]. Therefore, it is widely used in evaluating revascularization in the body. As shown in Fig. 9D, the blood vessels around the screw channel were stained with brown and had round or oval structures. 4- and 8- weeks post-operation, the A-H + AB-O and A-H + AB groups had more brown staining and wider distribution blood vessels than that of the control group and the A-H group. Moreover, according to the quantitative analysis (Fig. 9H), the CD31 positive area in the A-H + AB-O group (28.9 ± 2.854%) was larger than that in the control group (11.703 ± 2.204%), A-H group (8.907 ± 2.053%), and A-H + AB group (19.83 ± 2.873%), 8 weeks post-operation ($P < 0.05$ $n = 3$). Additionally, the CD31 positive area in the A-H + AB-O group was 1.39 times higher than that in the A-H + AB-O group, 4 weeks post-surgery.

Although the ovariectomized rat is one of the most commonly used models in medical research, further investigations on the large animal models are still needed. Moreover, we only used a fixed concentration of alendronate and bioactive glass based on the previous literature. The influence of different concentrations of alendronate and bioactive glass on bone formation in the screw channel will be explored in future studies. Furthermore, it is still unstudied whether the different concentrations of oxidized glucan will affect the hydrogel's capabilities in promoting osteogenesis and inhibiting osteoclast. Lastly, it is necessary to evaluate the abilities of hydrogel in adhesion and promoting angiogenesis *in vitro*.

Clinically, it is still challenged to treat the osteoporotic fracture because of the poor osteogenesis at the bone-implant interfaces. In this study, the organic-inorganic, double-adhesive hydrogel might simulate the adhesion of the chemical components of trabecular bone without significant influence on the osseointegration around the implants. It is a minimally invasive way for the implantations. In addition, it can decrease the financial burden providing a promising candidate for osteoporotic patients. Nonetheless, based on this work, further improvement is to be made on the current hydrogel due to its distance from a clinically competent one.

4. Conclusions

In this study, alendronate was grafted onto methacryloyl hyaluronic acid by activating the carboxyl group of methacryloyl hyaluronic acid. This graft was combined with BG modified by oxidized dextran, and UV crosslinking was used to cure the hybrid material in the cancellous bone area around implants, resulting in an injectable "organic/inorganic double-bonding hydrogel" that could regulate local bone metabolism and fix orthopedic implants under osteoporotic conditions. This double-adhesive hydrogel bonded not only with inorganic calcium phosphate on trabecular bone but also with organic collagen on trabecular bone. Meanwhile, the R2 side chains in alendronate can increase the anti-resorptive efficiency by inhibiting the mevalonate pathway. Moreover, a bone-like apatite layer was generated on the surface of the bioactive glasses after a series of interface reactions. These two effects balanced the bone metabolism around the implants with increased osseointegration. This organic-inorganic, double-adhesive composite hydrogel was an emerging treatment with limited cytotoxicity *in vitro*. It simulated the adhesion capability of the chemical components in the trabecular bone without losing osseointegration ability and biocompatibility. This hybrid hydrogel could be a promising candidate for effectively fixing the implants in patients with osteoporosis.

Declaration of competing interest

The authors declare no conflict of interest.

CRediT authorship contribution statement

Wei Jiang: Methodology, Investigation, Data curation, Formal analysis, Visualization, Writing – original draft. **Fushan Hou:** Investigation, Data curation, Validation, Visualization. **Yong Gu:** Methodology, Investigation, Data curation. **Qimanguli Saiding:** Formal analysis. **Pingping Bao:** Validation, Software. **Jincheng Tang:** Investigation. **Liang Wu:** Methodology, Software. **Chunmao Chen:** Investigation. **Cailiang Shen:** Conceptualization, Visualization. **Catarina Leite Pereira:** Writing – review & editing. **Marco Sarmento:** Writing – review & editing, Formal analysis, Visualization. **Bruno Sarmento:** Conceptualization, Writing – review & editing, Supervision, Funding acquisition. **Wenguo Cui:** Conceptualization, Methodology, Writing – review & editing, Supervision, Project administration, Funding acquisition. **Liang Chen:** Methodology, Writing – review & editing, Supervision, Project

administration, Funding acquisition.

Acknowledgements

This work was supported by the National Key R&D Program of China (2020YFA0908200), National Natural Science Foundation of China (82120108017), Six talent peaks project in Jiangsu Province (WSW-018). This work was financed by Portuguese funds through FCT - Fundação para a Ciência e a Tecnologia/Ministério da Ciência, Tecnologia e Ensino Superior in the framework of the project "Institute for Research and Innovation in Health Sciences" UID/BIM/04293/2019.

Appendix A. Supplementary data

Supplementary data to this article can be found online at https://doi.org/10.1016/j.bioactmat.2021.10.017.

References

[1] Z. Liu, M. Tang, J. Zhao, R. Chai, J. Kang, Looking into the future: toward advanced 3D biomaterials for stem-cell-based regenerative medicine, Adv. Mater. 30 (2018), e1705388.
[2] J.L. Wang, J.K. Xu, C. Hopkins, D.H. Chow, L. Qin, Biodegradable magnesium-based implants in orthopedics-a general review and perspectives, Adv. Sci. 7 (2020) 1902443.
[3] J. Li, Y. Long, F. Yang, H. Wei, Z. Zhang, Y. Wang, J. Wang, C. Li, C. Carlos, Y. Dong, Y. Wu, W. Cai, X. Wang, Multifunctional artificial artery from direct 3D printing with built-in ferroelectricity and tissue-matching modulus for real-time sensing and occlusion monitoring, Adv. Funct. Mater. 30 (2020).
[4] H. Yang, B. Jia, Z. Zhang, X. Qu, G. Li, W. Lin, D. Zhu, K. Dai, Y. Zheng, Alloying design of biodegradable zinc as promising bone implants for load-bearing applications, Nat. Commun. 11 (2020) 401.
[5] M. Vatankhah-Varnosfaderani, W. Daniel, M.H. Everhart, A.A. Pandya, H. Liang, K. Matyjaszewski, A.V. Dobrynin, S.S. Sheiko, Mimicking biological stress-strain behaviour with synthetic elastomers, Nature 549 (2017) 497–501.
[6] C. Hu, D. Ashok, D.R. Nisbet, V. Gautam, Bioinspired surface modification of orthopedic implants for bone tissue engineering, Biomaterials 219 (2019) 119366.
[7] L. Tan, J. Li, X. Liu, Z. Cui, X. Yang, S. Zhu, Z. Li, X. Yuan, Y. Zheng, K. Yeung, H. Pan, X. Wang, S. Wu, Rapid biofilm eradication on bone implants using red phosphorus and near-infrared light, Adv.Mater. 30 (2018), e1801808.
[8] L. Jiang, W. Zhang, L. Wei, Q. Zhou, G. Yang, N. Qian, Y. Tang, Y. Gao, X. Jiang, Early effects of parathyroid hormone on vascularized bone regeneration and implant osseointegration in aged rats, Biomaterials 179 (2018) 15–28.
[9] Y. Park, E. Cheong, J.G. Kwak, R. Carpenter, J.H. Shim, J. Lee, Trabecular bone organoid model for studying the regulation of localized bone remodeling, Sci Adv 7 (2021).
[10] S.L. Teitelbaum, Bone resorption by osteoclasts, Science 289 (2000) 1504–1508.
[11] Z. Geng, L. Ji, Z. Li, J. Wang, H. He, Z. Cui, X. Yang, C. Liu, Nano-needle strontium-substituted apatite coating enhances osteoporotic osseointegration through promoting osteogenesis and inhibiting osteoclastogenesis, Bioact Mater 6 (2021) 905–915.
[12] Z. Yang, Y. Xi, J. Bai, Z. Jiang, S. Wang, H. Zhang, W. Dai, C. Chen, Z. Gou, G. Yang, C. Gao, Covalent grafting of hyperbranched poly-L-lysine on Ti-based implants achieves dual functions of antibacteria and promoted osteointegration in vivo, Biomaterials 269 (2021) 120534.
[13] S. Lin, G. Yang, F. Jiang, M. Zhou, S. Yin, Y. Tang, T. Tang, Z. Zhang, W. Zhang, X. Jiang, A magnesium-enriched 3d culture system that mimics the bone development microenvironment for vascularized bone regeneration, Adv. Sci. 6 (2019) 1900209.
[14] D.M. Black, C.J. Rosen, Clinical practice. postmenopausal osteoporosis, N. Engl. J. Med. 374 (2016) 254–262.
[15] W. Yuan, Z. Li, X. Xie, Z.Y. Zhang, L. Bian, Bisphosphonate-based nanocomposite hydrogels for biomedical applications, Bioact Mater 5 (2020) 819–831.
[16] Y. Gao, S. Zou, X. Liu, C. Bao, J. Hu, The effect of surface immobilized bisphosphonates on the fixation of hydroxyapatite-coated titanium implants in ovariectomized rats, Biomaterials 30 (9) (2009) 1790–1796.
[17] U. Kettenberger, J. Ston, E. Thein, P. Procter, D.P. Pioletti, Does locally delivered zoledronate influence peri-implant bone formation? - spatio-temporal monitoring of bone remodeling in vivo, Biomaterials 35 (2014) 9995–10006.
[18] J. Chen, D. Wang, L.H. Wang, W. Liu, A. Chiu, K. Shariati, Q. Liu, X. Wang, Z. Zhong, J. Webb, R.E. Schwartz, N. Bouklas, M. Ma, An adhesive hydrogel with "load-sharing" effect as tissue bandages for drug and cell delivery, Adv. Mater. 32 (2020), e2001628.
[19] X. Mao, R. Cheng, H. Zhang, J. Bae, L. Cheng, L. Zhang, L. Deng, W. Cui, Y. Zhang, H.A. Santos, X. Sun, Self-healing and injectable hydrogel for matching skin flap regeneration, Adv. Sci. 6 (2019) 1801555.
[20] H. Madry, L. Gao, A. Rey-Rico, J.K. Venkatesan, K. Müller-Brandt, X. Cai, L. Goebel, G. Schmitt, S. Speicher-Mentges, D. Zurakowski, M.D. Menger, M.W. Laschke, M. Cucchiarini, Thermosensitive hydrogel based on PEO-PPO-PEO poloxamers for a controlled in situ release of recombinant adeno-associated viral vectors for effective gene therapy of cartilage defects, Adv. Mater. 32 (2020), e1906508.
[21] Y. Zeng, M. Zhou, L. Chen, H. Fang, S. Liu, C. Zhou, J. Sun, Z. Wang, Alendronate loaded graphene oxide functionalized collagen sponge for the dual effects of osteogenesis and anti-osteoclastogenesis in osteoporotic rats, Bioact Mater 5 (2020) 859–870.
[22] H. Quan, Y. He, J. Sun, W. Yang, W. Luo, C. Dou, F. Kang, C. Zhao, J. He, X. Yang, S. Dong, H. Jiang, Chemical Self-assembly of multifunctional hydroxyapatite with a coral-like nanostructure for osteoporotic bone reconstruction, ACS Appl. Mater. Interfaces 10 (2018) 25547–25560.
[23] K. Zhang, S. Lin, Q. Feng, C. Dong, Y. Yang, G. Li, L. Bian, Nanocomposite hydrogels stabilized by self-assembled multivalent bisphosphonate-magnesium nanoparticles mediate sustained release of magnesium ion and promote in-situ bone regeneration, Acta Biomater. 64 (2017) 389–400.
[24] H.S. Alghamdi, R. Bosco, S.K. Both, M. Iafisco, S.C. Leeuwenburgh, J.A. Jansen, J. J. van den Beucken, Synergistic effects of bisphosphonate and calcium phosphate nanoparticles on peri-implant bone responses in osteoporotic rats, Biomaterials 35 (2014) 5482–5490.
[25] J.M. Townsend, E.C. Beck, S.H. Gehrke, C.J. Berkland, M.S. Detamore, Flow behavior prior to crosslinking: the need for precursor rheology for placement of hydrogels in medical applications and for 3D Bioprinting, Prog. Polym. Sci. 91 (2019) 126–140.
[26] D. Seliktar, Designing cell-compatible hydrogels for biomedical applications, Science 336 (2012) 1124–1128.
[27] Y. Zhang, Y. Hu, Z. Luo, X. Shen, C. Mu, K. Cai, Simultaneous delivery of BMP-2 factor and anti-osteoporotic drugs using hyaluronan-assembled nanocomposite for synergistic regulation on the behaviors of osteoblasts and osteoclasts in vitro, J. Biomater. Sci. Polym. Ed. 26 (2015) 290–310.
[28] M. Diba, J. An, S. Schmidt, M. Hembury, D. Ossipov, A.R. Boccaccini, S. C. Leeuwenburgh, Exploiting bisphosphonate-bioactive-glass interactions for the development of self-healing and bioactive composite hydrogels, Macromol. Rapid Commun. 37 (2016) 1952–1959.
[29] J. Bai, H. Wang, H. Chen, G. Ge, M. Wang, A. Gao, L. Tong, Y. Xu, H. Yang, G. Pan, P.K. Chu, D. Geng, Biomimetic osteogenic peptide with mussel adhesion and osteoimmunomodulatory functions to ameliorate interfacial osseointegration under chronic inflammation, Biomaterials 255 (2020) 120197.
[30] B. Balakrishnan, D. Soman, U. Payanam, A. Laurent, D. Labarre, A. Jayakrishnan, A novel injectable tissue adhesive based on oxidized dextran and chitosan, Acta Biomater. 53 (2017) 343–354.
[31] T. Xin, Y. Gu, R. Cheng, J. Tang, Z. Sun, W. Cui, L. Chen, Inorganic strengthened hydrogel membrane as regenerative periosteum, ACS Appl.Mater.interfaces 9 (2017) 41168–41180.
[32] S. Feng, Z.X. Wu, Z. Zhao, J. Liu, K. Sun, C. Guo, H. Wang, Z. Wu, Engineering of bone- and CD44-dual-targeting redox-sensitive liposomes for the treatment of orthotopic osteosarcoma, ACS Appl.Mater.interfaces11 (2019) 7357–7368.
[33] R.H. Abou-Saleh, M.C. Hernandez-Gomez, S. Amsbury, C. Paniagua, M. Bourdon, S. Miyashima, Y. Helariutta, M. Fuller, T. Budtova, S.D. Connell, M.E. Ries, Y. Benitez-Alfonso, Interactions between callose and cellulose revealed through the analysis of biopolymer mixtures, Nat. Commun. 9 (2018) 4538.
[34] L. Gao, Y. Zhou, J. Peng, C. Xu, Q. Xu, M. Xing, J. Chang, A novel dual-adhesive and bioactive hydrogel activated by bioglass for wound healing, NPG Asia Mater. 11 (2019) 66.
[35] L. Xu, S. Gao, R. Zhou, F. Zhou, Y. Qiao, D. Qiu, Bioactive pore-forming b one adhesives facilitating cell ingrowth for fracture healing, Adv. Mater. 32 (2020), e1907491.
[36] L. Wu, Y. Gu, L. Liu, J. Tang, J. Mao, K. Xi, Z. Jiang, Y. Zhou, Y. Xu, L. Deng, L. Chen, W. Cui, Hierarchical micro/nanofibrous membranes of sustained releasing VEGF for periosteal regeneration, Biomaterials 227 (2020) 119555.
[37] Q. Wei, A. Holle, J. Li, F. Posa, F. Biagioni, O. Croci, A.S. Benk, J. Young, F. Noureddine, J. Deng, M. Zhang, G.J. Inman, J.P. Spatz, S. Campaner, E. A. Cavalcanti-Adam, BMP-2 signaling and mechanotransduction synergize to drive osteogenic differentiation via YAP/TAZ, Adv. Sci. 7 (2020) 1902931.
[38] K. Matsuoka, L. Bakiri, L.I. Wolff, M. Linder, A. Mikels-Vigdal, A. Patiño-García, F. Lecanda, C. Hartmann, M. Sibilia, E.F. Wagner, Wnt signaling and loxl2 promote aggressive osteosarcoma, Cell Res. 30 (2020) 885–901.
[39] R. Agarwal, C. González-García, B. Torstrick, R.E. Guldberg, M. Salmerón-Sánchez, A.J. García, Simple coating with fibronectin fragment enhances stainless steel screw osseointegration in healthy and osteoporotic rats, Biomaterials 63 (2015) 137–145.
[40] Y. Wei, Z. Liu, X. Zhu, L. Jiang, W. Shi, Y. Wang, N. Xu, F. Gang, X. Wang, L. Zhao, J. Lin, X. Sun, Dual directions to address the problem of aseptic loosening via electrospun PLGA @ aspirin nanofiber coatings on titanium, Biomaterials 257 (2020) 120237.
[41] H. Zhao, Y. Huang, W. Zhang, Q. Guo, W. Cui, Z. Sun, D. Eglin, L. Liu, G. Pan, Q. Shi, Mussel-inspired peptide coatings on titanium implant to improve osseointegration in osteoporotic condition, ACS Biomater. Sci. Eng. 4 (2018) 2505–2515.
[42] W. Zhao, D. Michalik, S. Ferguson, W. Hofstetter, J. Lemaître, B. von Rechenberg, P. Bowen, Rapid evaluation of bioactive Ti-based surfaces using an in vitro titration method, Nat. Commun. 10 (2019) 2062.
[43] X. Wang, L. Gao, Y. Han, M. Xing, C. Zhao, J. Peng, J. Chang, Silicon-enhanced adipogenesis and angiogenesis for vascularized adipose tissue engineering, Adv. Sci. 5 (2018) 1800776.
[44] D. Cogswell, M. Sun, E. Greenberg, C.E. Margo, E.M. Espana, Creation and grading of experimental corneal scars in mice models, Ocul. Surf. 19 (2021) 53–62.